

A phase diagram of the pinch-off behavior of impulsively-induced viscoelastic liquid jets

Asuka Hosokawa,[†] Kyota Kamamoto,[†] Hiroya Watanabe,[†] Hiroaki Kusuno,[†]
Kazuya U. Kobayashi,[‡] and Yoshiyuki Tagawa^{*,†}

[†]*Department of Mechanical Systems Engineering, Tokyo University of Agriculture and Technology, Naka-cho 2-24-16, Koganei, Tokyo, 184-8588, Japan*

[‡]*Department of Mechanical Engineering, Nippon Institute of Technology, Gakuendai 4-1, Miyashiro-machi, Minamisaitama-gun, Saitama, 345-8501, Japan*

E-mail: tagawayo@cc.tuat.ac.jp

Abstract

In this study, we systematically investigate the behaviors of viscoelastic liquid jets using an impulsive force, particularly in the high velocity and high elasticity regimes. The resulting jets are categorized into two types: (i) pinch-off jets, which break up during elongation after ejection, and (ii) no-pinch-off jets, which either retract to the nozzle after maximum elongation, known as ‘bungee-jumper jets’ or return without elongation after ejection. We then propose criteria to delineate these regions using Reynolds number Re and Weissenberg number Wi , reflecting the initial conditions at the jet ejection and the solution’s rheological properties, respectively. We find that pinch-off jets occur at $Re \gtrsim 23.4Wi$ in high elasticity regimes ($Wi \gtrsim 10$), and at $Re \gtrsim 250$ in low elasticity regimes ($Wi \lesssim 10$). In addition, we demonstrate that the phase diagram of these behaviors can be rationalized through the focused jet modeling using the finitely extensible non-linear elastic dumbbell model with the Chilcott–Rallison closure approximation (FENE-CR).

Introduction

Liquid jets have been studied in the past from a variety of perspectives due to their significance in fundamental research and their widespread occurrence¹. A typical liquid jet is a focused jet in which the diameter of the jet tip is smaller than the diameter of the jet bottom.²⁻⁴ Focused jets are caused by solid spheres or droplets impinging on the surface of a liquid bath⁵ or by the formation of standing waves (Faraday waves) on the surface of a liquid bath⁶. It can also be caused by rapid acceleration of a concave gas-liquid interface by an impulsive force⁷. Such impulsively-induced focused jets are expected to be applied to needle-free injection of drugs⁸ and inkjet printing technology⁹ because of their thin tips¹⁰ and high speed.²

For inkjet printing applications, it is very important to understand the mechanisms of jet formation and breakup. The formation and breakup of Newtonian fluid jets is well known and predictable by considering Rayleigh-Plateau instability.¹¹ After pinch-off from the nozzle, the jet forms a single droplet or multiple droplets (satellite).¹² Since satellite generates unwanted droplets on the target substrate and degrade print quality, it is desirable for a single droplet to be formed during actual printing. Therefore, methods to generate a single droplet have been investigated.

One method is to increase the viscosity of the liquid. Delrot et al.¹³ showed that the condition for single droplet formation is expressed as $0.1 < Oh < 1$ using the Ohnesorge number, $Oh = \mu/\sqrt{\rho r \sigma}$, where μ is the liquid viscosity, ρ is the liquid density, r is the characteristic length scale for the flow of interest, and σ is the liquid-air surface tension. Another way is to add polymers to the liquid to give it viscoelastic properties. Viscoelastic liquid jets exhibit a characteristic phenomenon called ‘beads-on-a-string’, in which droplets and strings of liquid form a series of beads, suppressing breakup.¹⁴ Previous studies have shown that the addition of small amounts of high molecular weight polymers to liquids suppresses satellite formation.¹⁵ Conversely, when large amounts of high molecular weight polymers are added, elasticity can delay or prevent jet formation from the nozzle. The

characteristic jet produced in this case is called a ‘bungee-jumper jet’, which extends to its maximum length after formation and then gets pulled back to the gas-liquid interface without pinch-off.¹⁶ In order to determine the ideal amount of polymer to add, jet behavior has been investigated by varying the molecular weight and concentration of polymers in drop-on-demand (DoD) printing, a common inkjet technology. Jet behavior has been classified by experiments^{15,17–19} and simulations,^{16,20} mainly using polymer concentration and molecular weight. Physical considerations have also been made on the influence of viscoelasticity on jet behavior by modeling the phenomena using viscoelastic models.^{15,17–19} In another nozzle-less printing technique called blister-actuated laser induced forward transfer (BA-LIFT), Turkoz et al.²¹ experimentally investigated the conditions under which a single droplet is formed after jet formation and found that the Deborah number, De , and the Ohnesorge number, Oh , were used to predict droplet formation. Here, $De = \lambda/t_c$, where λ is the liquid relaxation time and t_c is the characteristic time scale.

Although there is a growing number of research on inkjet printing of viscoelastic liquids,^{20,22–24} little is known about the influence of viscoelasticity in the inkjet technology of impulsively-induced focused jets. So far, Onuki et al.⁹ has investigated the low viscoelasticity regime and found that the theory of jet velocity in Newtonian fluids is applicable to low viscoelastic liquids. Franco-Gomez et al.²⁵ investigated highly viscoelastic jet behavior and found an increase in the maximum jet velocity due to elasticity. However, little physical understanding of the effect of viscoelasticity on the behavior of focused jets has been achieved in either of these investigations. Since a impulsively-induced focused jet technology can generate jets at high velocities,⁹ it is possible to investigate viscoelastic jet behavior at higher velocities than with conventional inkjet technology.

In this paper, we quantify the effect of viscoelasticity on pinch-off behavior at high velocities using impulsively induced focused jets. To this purpose, a systematic investigation is conducted by varying the magnitude of viscoelasticity over a wide range. The formation of viscoelastic jets is observed in detail with a high-speed camera, and the jet behavior is

classified into phase diagrams using the Reynolds number, Re , and the Weissenberg number, Wi . Here $Re = \rho U_0 r / \mu$, where U_0 is the characteristic velocity, and $Wi = \lambda U_0 / r$. The reason for adapting Re and Wi is discussed in “Results and Discussion” section. Furthermore, we will investigate whether the models proposed in DoD printing^{15,18} can be applied to viscoelastic focusing jets, and attempt to provide a physical interpretation of viscoelastic jet behavior.

Experimental Section

Impulsively-induced focused jet generation

We use two different methods to vary the initial velocity of the fluid while considering a wide range of parameters. The first method generates jet using a test tube. This method allow us to generate highly controllable focused jet easily and covers the range of parameters within $0.06 < Wi < 120$ and $16 < Re < 5900$. The second method uses a double-layer narrow tube to generate jet that is capable of ejecting liquid with high elasticity, and also consider a wide parametric range that covers $3.3 < Wi < 16000$ and $24 < Re < 2700$.

Method I: Test tube impacting on a floor

A schematic of the experimental setup for method I is shown in Figure 1a. A test tube (A-16.5, Maruemu, inner diameter $2r = 14.3$ mm) is filled with liquid (liquid height, $L = 32$ mm) and suspended by an electromagnet at a dropping height, H . When the electromagnet is switched off, the test tube falls freely. When the test tube collides with the floor, the liquid is accelerated over a very short time, and as a result, an upward oriented focused liquid jet is formed from the gas-liquid interface.^{26,27}

In this experiment, the initial velocity of the fluid U_0 is controlled by varying the drop height of the test tube ($H = 3\text{--}300$ mm) and the floor material (SS400, nitrile rubber). U_0 is the velocity of the gas-liquid interface just after the impact, and is the sum of the falling

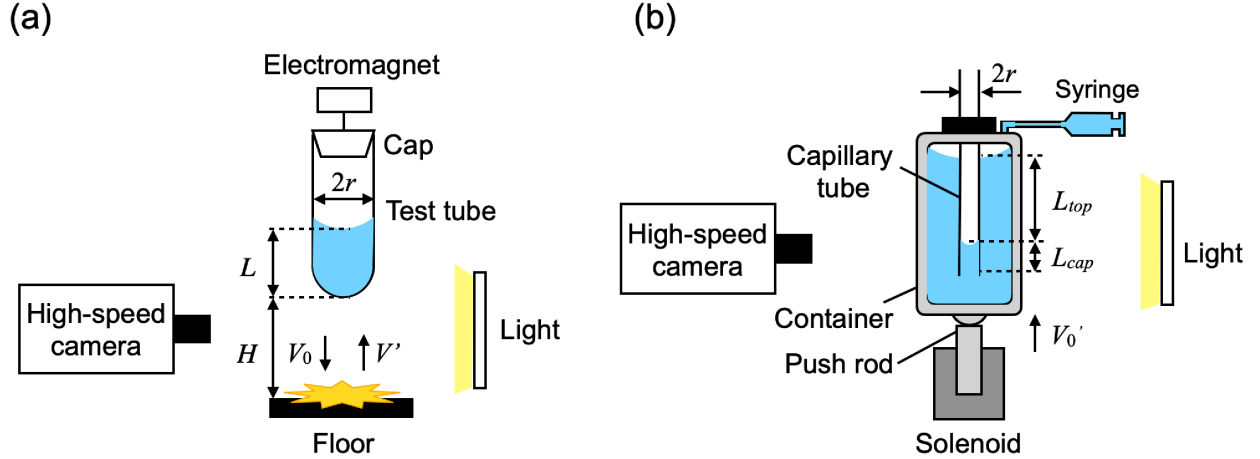


Figure 1: The experimental setup for generating a focused jet using (a) a falling test tube, and (b) double-layer narrow tube, where the capillary tube placed inside the container with the liquid level inside the tube set deeper than that of outside the tube.

velocity of the test tube (velocity just before impact) V_0 and the rebound velocity relative to the floor V' , expressed as in $U_0 = V_0 + V'$.⁴ In this case, V_0 is given by $V_0 = \sqrt{2gH}$, which is derived from the energy conservation law, where g is the gravitational acceleration. V' is given by $V' = H'/t$, where H' is the rebound velocity of the test tube 10 ms after impact ($t = 0$ ms). The jet formation is captured using a high-speed camera (FASTCAM SA-X, Photron) and a backlight (White Led Backlight, Phlox) at 30,000 fps.

Method II: Double-layer narrow tube

A schematic of the experimental setup for method II is shown in Figure 1b. We use an ejection device with a capillary tube to generate jets using the impulsive force.⁹ In this experiment, a glass capillary tube (Fuji Science Industry, inner diameter $2r = 2$ mm) is inserted into a container partially filled with liquid and sealed outside the tube. We control the pressure of the sealed air outside the tube using a syringe in order to push the liquid interface inside the capillary near to the bottom of the container and thus change the position of the liquid surface inside the capillary L_{cap} . The liquid level inside the tube is kept deeper than that outside the tube. An electromechanical device (ShinDengen solenoids, KGK power supply) is used to apply a vertical upward impulsive force at a velocity V'_0 . The liquid inside the

Table 1: The physical properties of the solutions

Solutions		Density ρ [kg/m ³]	Surface tension σ [mN/m]	Relaxation time λ [ms]
PEO	0.4M 1wt%	999.7	64.0	1.9
	2M 1wt%	998.3	64.1	12.4
	5M 0.5wt%	996.4	62.8	35.4
	5M 1wt%	998.0	62.0	57.2
	8M 1wt%	981.4	60.6	207.6
	8M 2wt%	999.1	62.1	301.4
PAM	5-6M 0.2wt%	995.2	72.5	3.3
	5-6M 0.4wt%	1002.8	63.0	4.6
	5-6M 0.8wt%	1000.0	71.0	16.5
	5-6M 0.4wt% (G70W30)	1176.9	66.4	91.0

tube is rapidly accelerated and a focused jet is generated from the inside of the tube. The initial velocity U_0 of the generated jet varies depending on the ratio of the distance between the gas-liquid interface outside the tube L_{top} and the liquid surface position inside the tube L_{cap} . The initial velocity U_0 is calculated using the following equation:⁹

$$U_0 = \frac{L_{top}}{L_{cap}} V_0' \quad (1)$$

The jet formation is captured using a high-speed camera and a backlight at 30,000–60,000 fps.

Properties of the liquid solutions

Polymer solutions were used as the viscoelastic liquids in the experiments (Table 1). We used two types of polymers: polyethylene oxide (Sigma-Aldrich, molecular weight $M_w = 0.4, 2, 5,$ and 8 M (= million), polymer concentration $c = 0.5, 1,$ and 2 wt%) and polyacrylamide (Sigma-Aldrich, $M_w = 5\text{--}6$ M, $c = 0.2, 0.4,$ and 0.8 wt%). The solutions were prepared by adding polyethylene oxide (PEO) and polyacrylamide (PAM) to pure water and aqueous-glycerin solution (glycerol: 70 wt%, water: 30 wt%, G70W30) as solvents and stirring at 650 rpm, 60 °C for 24 to 48 hours.

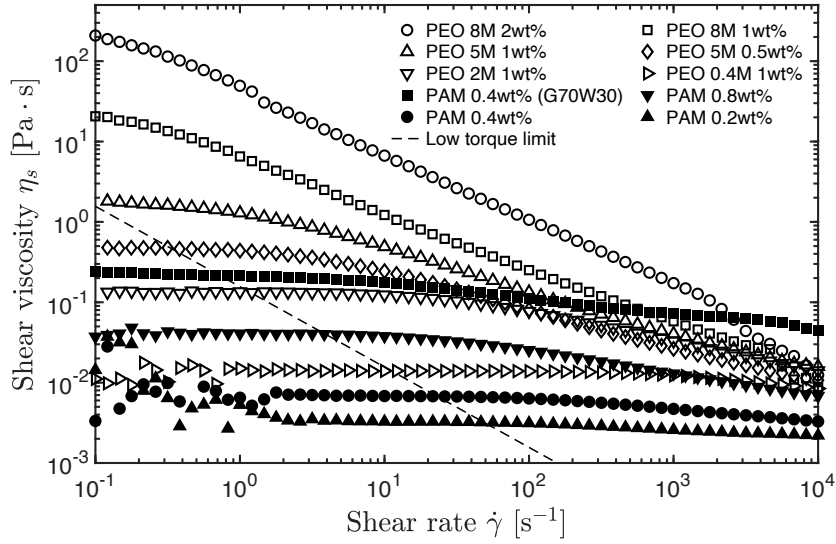


Figure 2: The shear viscosity for the PEO and PAM solutions.

Polymer solutions generally exhibit shear-thinning behavior, in which the viscosity decreases with an increasing strain rate. The shear viscosities of the PEO and PAM solutions as measured with a shear rheometer (MCR-302, Anton Paar) are shown in Figure 2. The dashed line in Figure 2 represents the low torque limit of the measured shear viscosity due to the torque sensitivity of the shear rheometer.²⁸ From Figure 2, the shear viscosity μ_s of both the PEO and PAM solutions decreases with an increasing shear rate $\dot{\gamma}$, indicating shear-thinning properties. In both solutions, the higher the molecular weight and concentration, the greater the shear viscosity and the greater the slope of the shear curve. The higher the molecular weight and concentration, the greater the viscoelasticity and thus, the stronger the shear-thinning property.²⁹

Viscoelastic liquids also have spring-like elastic properties. We use the relaxation time λ as a physical property to express the magnitude of the elasticity. We estimate λ using dripping-onto-substrate capillary breakup elongation rheometry (DoS-CaBER), which is a method for evaluating the extensional rheology of viscoelastic liquids.³⁰ This method enables the measurement of the relaxation times of low-viscoelastic liquids, which are difficult to measure with rheometers.^{31,32} Figure 3a shows the experimental DoS-CaBER setup. First,

the sample is pushed out of a syringe to form a droplet at the tip of the nozzle (outer diameter $2R_0 = 1.27$ mm, inner diameter $2R_i = 0.97$ mm). When the droplet adheres to the glass plate with its own weight, the liquid spreads on the glass plate and forms a liquid thread due to the surface tension. The liquid thread becomes thin and shreds gradually. The force that resists the surface tension acting on the liquid thread differs depending on the solution, and the elastic force is dominant in viscoelastic liquids (in the elasto-capillary regime).³³ The time evolution equation of the liquid thread radius R formed in this case is expressed as

$$\frac{R(t)}{R_0} \propto \exp\left(-\frac{t}{3\lambda}\right). \quad (2)$$

where R_0 is the nozzle radius and t is the time since the liquid thread was formed.³⁴ Therefore, the relaxation time λ of the sample can be calculated from the time evolution of the liquid thread radius R .

An example analysis of the liquid relaxation time λ using DoS-CaBER is shown in Figure 3b. The horizontal axis is the time t and the vertical axis is the dimensionless liquid thread radius R/R_0 , which is the liquid thread radius R divided by the nozzle radius R_0 . The plot shows a 5M 1wt% PEO solution. Since the extension rate is constant in the elasto-capillary regime,³⁵ the extension rate is calculated from the DoS-CaBER experimental results and the elasto-capillary regime is determined. An exponential approximation is made in this region, and the relaxation time λ is derived using Eq 2. relaxation time λ is derived using Eq. 2.

The relaxation times λ for the PEO and PAM solutions are calculated using the same procedure and the results are shown in Table 1. The relaxation time λ increases with an increasing concentration c and molecular weight M_w for both the PEO and PAM solutions. Our results are consistent with previous studies.²⁹ In addition, when comparing 2M 1wt% and 5M 0.5wt% PEO solutions, λ is larger for 5M 0.5wt%. This is because the molecular weight M_w makes a larger contribution to the relaxation time λ than the concentration c .¹⁷

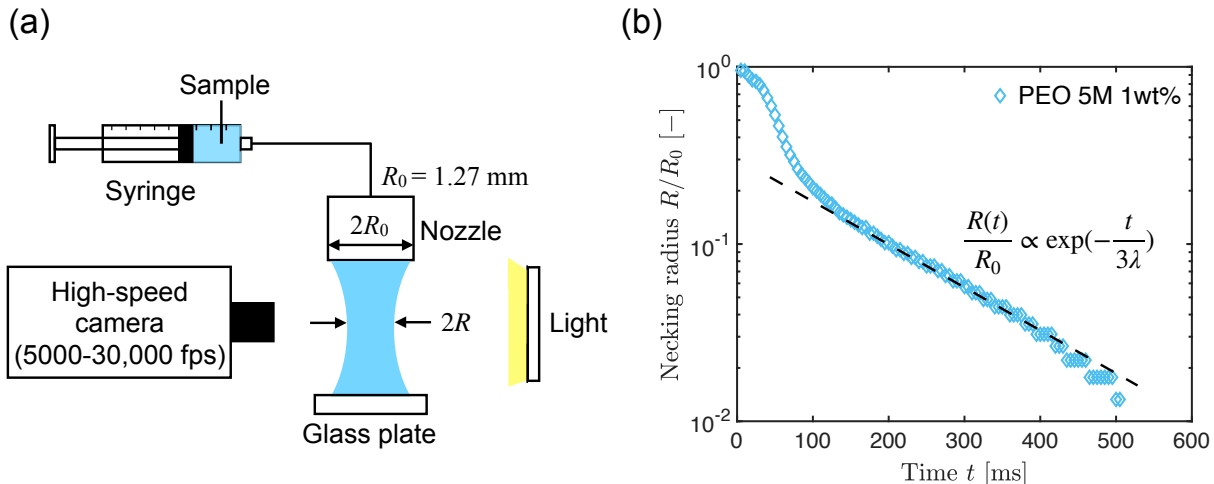


Figure 3: (a) The experimental setup for the dripping-onto-substrate capillary breakup extensional rheometry: DoS-CaBER. (b) The non-dimensional radius (the ratio of the neck radius to the nozzle radius) as a function of time for 5M 1wt% PEO is shown on a semi-log plot. The dashed lines shows the fitted region obtained using Eq. 2.

Results and Discussion

In our experiment, we have identified two different types of jets through systematic experiments by varying the magnitude of the viscoelasticity and initial velocity.

The typical behaviors of the generated viscoelastic liquid jets are shown in Figure 4. Note that the time of the test tube impacting the floor is used as the reference time ($t = 0$ ms), and the time evolution of the jet from that point is shown in Figure 4. Figure 4a shows images of a jet generated by the ejection of a 0.4M 1wt% PEO solution at an initial velocity of $U_0 = 0.84$ m/s. The jet ejected from the interface has a shape in which the tip diameter is smaller than the tail diameter, indicating that it is a focused jet. After ejection, the focused jet is elongated vertically upward, and the tip is pinched off at $t = 63$ ms. Thus, we define this type of jet as a ‘pinch-off jet’. Figure 4b shows images of a jet generated by ejecting a 5M 1 wt% PEO solution at an initial velocity of $U_0 = 2.9$ m/s. The focused jet is elongated after ejection from the interface and reaches its maximum length 32 mm at $t = 23$ ms. After that, the jet returns to the initial interface. It should be noted that the jet is prevented from being pinched off despite the large impact force applied in Figure 4b

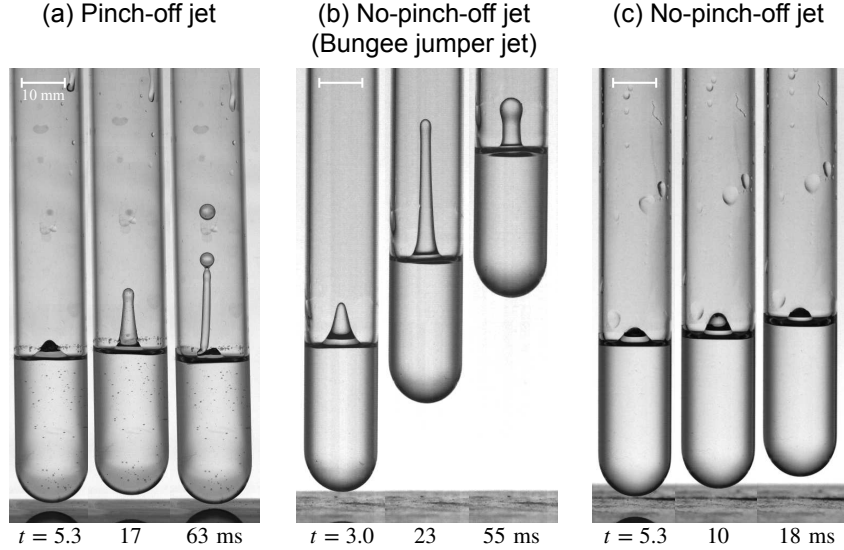


Figure 4: Viscoelastic liquid jets can be divided into two typical types: (a) pinch-off jets and (b)(c) no-pinch-off jets. (a) Images of a jet generated by the ejection of a 0.4M 1wt% PEO solution at an initial velocity of $U_0 = 0.84$ m/s corresponding to the Supporting Information 1. The jet is ejected from the interface and extends vertically upward, and the tip is pinched off after a certain time. (b) Images of a jet generated by the ejection of an 5M 1wt% PEO solution at an initial velocity of $U_0 = 2.9$ m/s corresponding to the Supporting Information 2. The jet is elongated after ejection from the interface and, after maximum elongation, pulled back to the initial interface. (c) Images of a jet generated by the ejection of a 8M 1wt% PEO solution at an initial velocity of $U_0 = 1.2$ m/s corresponding to the Supporting Information 3. The jet is ejected from the interface but returns to the initial interface without elongation.

compared to that in Figure 4a. This phenomenon was also observed in a previous study as a ‘bungee-jumper jet’ when the elasticity of the solution is large,²⁵ and it is believed that the elastic force contributes to the pulling back of the jet. We define such a jet that pulls back to the initial interface after maximum elongation as a ‘no-pinch-off jet (bungee-jumper jet)’. Finally, Figure 4c shows images of a jet generated by ejecting an 8M 1 wt% PEO solution at an initial velocity of $U_0 = 1.2$ m/s. The jet is ejected from the interface but returns to the initial interface without elongation. The reason for this is presumed to be that the initial velocity is smaller in Figure 4c than in Figure 4b, i.e., the jet is not given a sufficient impulsive force to generate a jet. Such jets are also defined as ‘no-pinch-off jets’.

These changes in jet behavior are considered to be caused by the balance between the inertial force and the viscoelasticity of the liquid that dominates during jet extension. We

organize our results in terms of two dimensionless numbers. One is the Reynolds number Re , which represents the ratio of the inertial force to the viscous force, and is defined as

$$Re = \frac{\rho U_0 r}{\mu_s}, \quad (3)$$

where ρ is the density of the solution. Since the polymer solution used in this experiment has shear-thinning properties, we calculate the strain rate $\dot{\gamma}$ from the elongation behavior of the jet ($\dot{\gamma} = O(10^2-10^3)$) and assume the shear viscosity μ_s at that strain rate as the representative viscosity. The other is the Weissenberg number Wi , which represents the ratio of the elastic force to the viscous force, and is defined as

$$Wi = \frac{\lambda U_0}{r}. \quad (4)$$

We adapt Re and Wi instead of other dimensionless numbers because they are directly derived from the equations of motion of viscoelastic jet discussed later in this paper.

The results of organizing the jet behaviors using the Reynolds number Re and the Weissenberg number Wi are shown in Figure 5. The error bars in Figure 5 indicate the error range associated with the estimation of the shear viscosity μ_s . The higher the viscoelasticity of the liquid, the greater the shear-thinning property, resulting in a larger error especially in the region of high Wi .

Figure 5 shows that the jet behavior can be divided into two regions, pinch-off, and no-pinch-off jets, depending on Re and Wi . The fact that the results can be organized by parameters related to the initial conditions of jet ejection and the physical properties of the solution suggests that these parameters have a significant effect on the behavior of the viscoelastic liquid jets. Furthermore, the experimental results are distributed in a unified manner regardless of the type of polymer (PEO or PAM). Therefore, we believe the effect of the polymer type on the jet behavior is small. In the high Wi region, the elasticity of the solution affects the jet behavior, but in the low Wi region, it has little effect on the jet

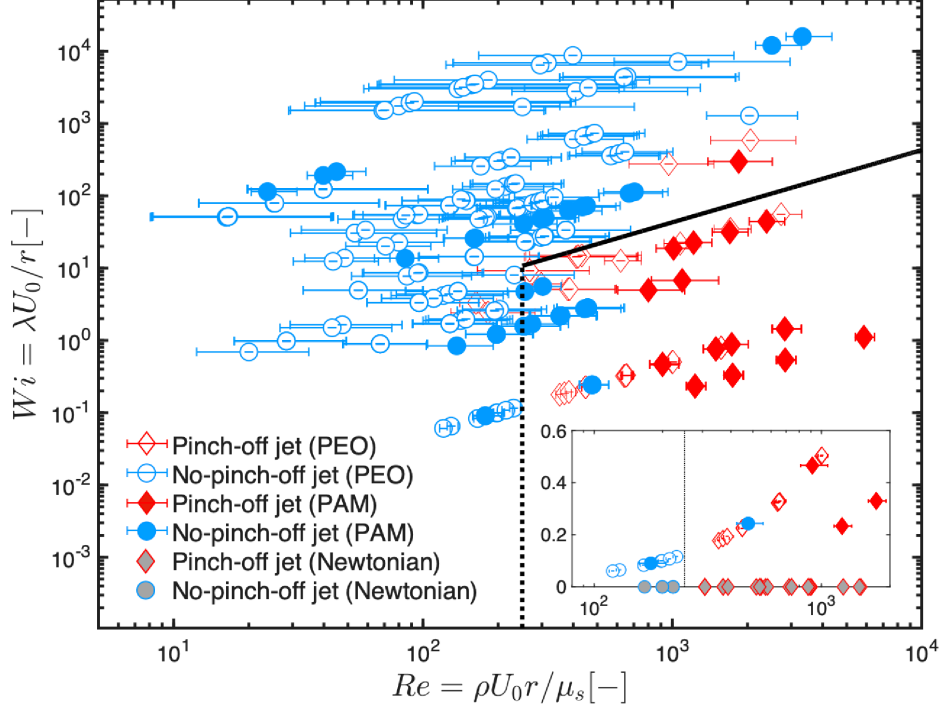


Figure 5: A phase diagram of the impulsively-induced jet behavior of viscoelastic liquids with a Weissenberg number Wi and Reynolds number Re . The outer frame of the plot indicates the jet type: red indicates a pinch-off jet and blue indicates a no-pinch-off jet. The markers in the plot indicate the type of solution: an open markers indicates PEO solutions, markers filled with blue and red indicate PAM solutions, and gray markers indicate an aqueous-glycerin solution, which is a Newtonian fluid (See Figure 7 for the jet behavior of the Newtonian liquid). The inset shows the region with low Wi ($Wi \leq 0.6$).

behavior and the jet is considered to behave like a Newtonian fluid. Thus, in the following, we will discuss the jet behavior in detail in two regions: 1) the region with $Wi \gtrsim 10$ and 2) the region with $Wi \lesssim 10$.

The region with $Wi \gtrsim 10$ (Elastic dominated)

Figure 5 shows that in the region with $Wi \gtrsim 10$, a no-pinch-off jet occurs in the region with high Wi , and a pinch-off jet occurs in the region with low Wi . It should be noted that even for a sufficiently high Re , $Re \gtrsim O(10^3)$, the pinch-off of the jet is inhibited in the region with high Wi ($Wi \gtrsim O(10^3)$). The pinch-off phenomenon is suppressed even in this

region, which is a region of high velocity and high viscoelasticity compared to the range of previous studies on inkjet of viscoelastic liquids.^{16,23} The elasticity increases with increasing Wi , suggesting that bungee-jumper jets are caused by the elasticity of the viscoelastic liquids. Thus, remarkably, we find that the pinch-off is suppressed even in the high-velocity regimes when compared to the range of previous studies on inkjet applications using viscoelastic liquids^{16,23}.

To understand this phenomenon, we model a jet using a viscoelastic model following previous studies.^{15,18} The effect of elasticity on the jet behavior can be evaluated by introducing a constitutive equation that accounts for elastic stress.²⁰ There are various models, but here we use the finitely extensible non-linear elastic dumbbell model with the Chilcott–Rallison closure approximation, known as the FENE-CR model.³⁶ The FENE-CR model is one of the simple constitutive equations used for the rheological properties of dilute polymer solutions.

Assuming an incompressible fluid, the continuity equation and Navier–Stokes equation can be expressed using the fluid velocity \mathbf{u} , pressure p , and stress tensor $\boldsymbol{\sigma}$ as

$$\nabla \cdot \mathbf{u} = 0, \quad (5)$$

$$\rho \frac{D\mathbf{u}}{Dt} = -\nabla p + \nabla \cdot \boldsymbol{\sigma}. \quad (6)$$

In the FENE-CR model, the stress is given by

$$\boldsymbol{\sigma} = 2\mu_s \mathbf{E} + Gf(\mathbf{A} - \mathbf{I}), \quad (7)$$

where $\mathbf{E} = (\nabla \mathbf{u} + \nabla \mathbf{u}^T)/2$ is the strain rate tensor, G is the elastic modulus, \mathbf{I} is the unit matrix, \mathbf{A} is the conformation tensor related to the deformation of the polymer chains, and f is a nonlinear function that enforces finite extensibility. We note

$$\frac{D\mathbf{A}}{Dt} = \nabla \mathbf{u}^T \cdot \mathbf{A} + \mathbf{A} \cdot \nabla \mathbf{u} - \frac{f}{\lambda}(\mathbf{A} - \mathbf{I}). \quad (8)$$

Using the elongation limit of the polymer chain L , f is expressed as

$$f = (1 - tr(\mathbf{A})/L^2)^{-1}. \quad (9)$$

Since the tip of the jet is faster than the tail, we assume that the inertia at the tip of the jet affects the jet behavior, and propose a simple model as shown in Figure 6. This model is based on the model outlined by previous studies.^{15,18} Hoath et al.¹⁸ predicted from modeling that the maximum polymer concentration at which a jet of a certain speed can be formed scales with molecular weight, and demonstrated agreement with experimental data. Later, McIlroy et al.¹⁵ validated the predictions of the simple model of jets given by Hoath et al.¹⁸ against both experimental observations and numerical simulations and were able to identify all three asymptotic regions identified by Hoath et al.¹⁸ for low viscosity solvents. We define the initial condition to be $t = t_r$, where t_r is the time when the jet tip is ejected by a distance r (=tube radius) from the initial interface in Figure 6a. We set the initial condition to a value used by previous study.¹⁵ The jet velocity at this time is U_r . The jet then decelerates to a velocity U , and the jet tail deforms uniformly with time from an initial length r to z at time t (Figure 6b). The volume of fluid at the tip Ω_{tip} and at the tail Ω_{tail} are assumed to remain constant.

For this simple model, the velocity U is given by $U = dz/dt$. Assuming that the only

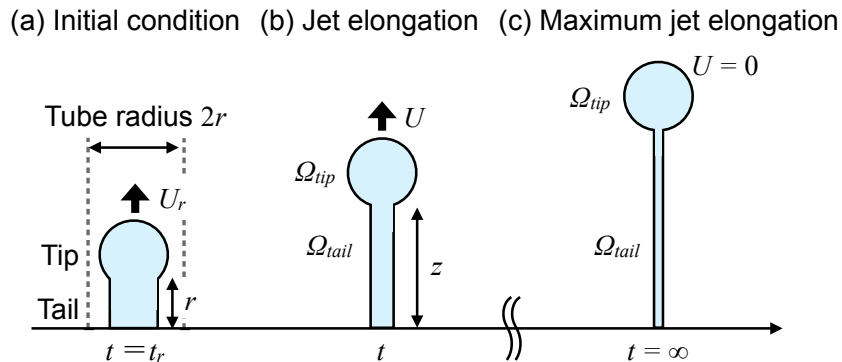


Figure 6: A simplified model of the viscoelastic jet.

forces acting on the jet tip are from the stress difference in the tail. The equation of motion of the tip is given by

$$\rho\Omega_{tip}\frac{dU}{dt} = -\frac{\Omega_{tail}}{z}\left(\frac{\mu_e U}{z} + Gf(A_{zz} - A_{rr})\right), \quad (10)$$

where μ_e is extensional viscosity.¹⁵ Assuming an axisymmetric flow, Eq. 8 can be expanded into an axial component A_{zz} and a radial component A_{rr} , and the orthogonal stresses A_{rz} and A_{zr} in the jet are neglected ($A_{rz} = A_{zr} = 0$). Thus, A_{zz} and A_{rr} can be expressed as follows:

$$\frac{dA_{zz}}{dt} = \left(\frac{2U}{z} - \frac{f}{\lambda}\right)A_{zz} + \frac{f}{\lambda}, \quad (11)$$

$$\frac{dA_{rr}}{dt} = -\left(\frac{U}{z} + \frac{f}{\lambda}\right)A_{rr} + \frac{f}{\lambda}. \quad (12)$$

Furthermore, assuming that the axial elongation of the polymer chain is sufficiently large ($A_{zz} \gg 1 \rightarrow f \sim 1$, $A_{zz} \gg A_{rr}$), we can write $A_{zz} \sim (z/r)^2 e^{-t/\lambda}$ and $A_{rr} \sim 0$. Therefore, the deceleration ΔU at position z ($z > r$) is obtained by integrating Eq. 10 at time t (Figure 6b).

$$\rho\Omega_{tip}\Delta U(z) = -\Omega_{tail}\left(\mu_e\left(\frac{1}{r} - \frac{1}{z}\right) + \frac{G}{r^2}\int_0^t ze^{-\frac{t}{\lambda}}dt\right). \quad (13)$$

By assuming that $\Delta U/U$ is small, $z = r + U_r t$, and taking the limit $t \rightarrow \infty$ following previous study,¹⁸ we can approximate the integral as

$$\int_0^\infty ze^{-\frac{t}{\lambda}}dt = \int_0^\infty (r + U_r t)e^{-\frac{t}{\lambda}}dt \sim U_r \lambda^2. \quad (14)$$

In addition, assuming $U = 0$ when $t \rightarrow \infty$ (Figure 6c), we get

$$\rho\Omega_{tip}U_r = \Omega_{tail}\left(\frac{\mu_e}{r} + \frac{U_r}{r^2}G\lambda^2\right). \quad (15)$$

When the elastic term is sufficiently large compared with the viscous term, Eq. 15 can be transformed into

$$\rho\Omega_{tip}U_r = \Omega_{tail}\frac{U_r}{r^2}G\lambda^2. \quad (16)$$

Assuming that the jet tip diameter d_{tip} and the tail diameter d_{tail} satisfy $d_{tip} \sim \alpha r$ and $d_{tail} \sim r$ in the initial state (Figure 6a), then $\Omega_{tip} \sim 4\pi(\alpha r/2)^3/3$, $\Omega_{tail} \sim \pi r^3/4$. We note that α is a constant. Furthermore, assuming $G \sim \mu_s/\lambda$ and $U_r \propto U_0$, and substituting these into Eq. 16, we obtain

$$Re \sim \frac{3}{2\alpha^3}Wi. \quad (17)$$

For $Re \lesssim 3/(2\alpha^3)Wi$, the jet is pulled back by the elastic force, resulting in a no-pinch-off jet, and for $Re \gtrsim 3/(2\alpha^3)Wi$, a pinch-off jet occurs due to the lack of elastic force. The experimental value of α is 0.4. From the above, we suggest that the threshold for the occurrence of pinch-off jets in the region of $Wi \gtrsim 10$ can be expressed by the following equation:

$$Re \gtrsim 23.4Wi. \quad (18)$$

The region with $Wi \lesssim 10$ (Viscous dominated)

From Figure 5, no-pinch-off jets are observed for $Re \lesssim 250$ the dashed vertical line, and pinch-off jets are observed for $Re \gtrsim 250$ when $Wi \lesssim 10$. This is considered to be because the elasticity of the solution has little effect on the jet behavior in the low Wi region, and the jet behaves like a Newtonian fluid. In a previous study, the effect of viscosity on the jet velocity of a Newtonian fluid was investigated.⁹ It was reported that a viscous boundary layer develops on the wall surface at $Re \lesssim 200$, which prevents the focusing effect of the flow. Therefore, the lower Re is in the present study, the more the viscous boundary layer

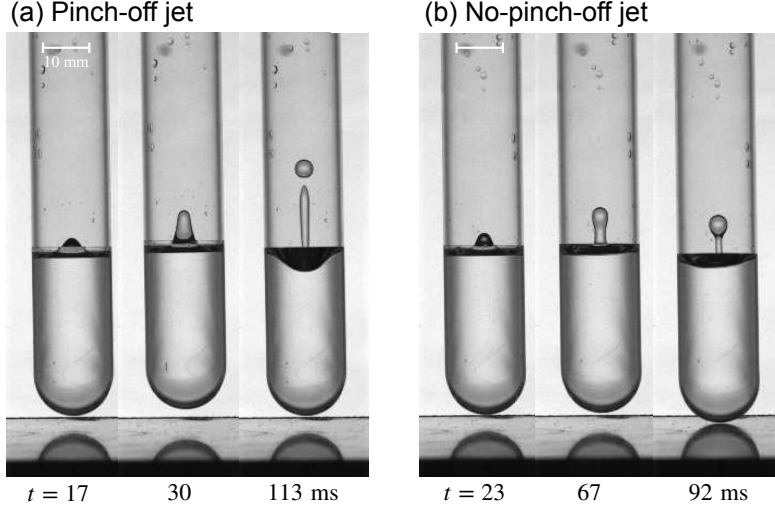


Figure 7: The jet behavior of aqueous-glycerin solution (G70W30). (a) A jet ejected from the interface and extended vertically upward, with the tip pinched off after a certain time when $Re \sim 370$. (b) A jet ejected from the interface but returned to the initial position without being pinched off when $Re \sim 230$.

develops on the wall surface and near the free surface, which prevents jet extension.

When the fluid behaves in a Newtonian Fluid-like manner ($\mu_e = 3\mu_s$) and viscosity is dominant, Eq. 15 can be transformed into

$$\rho\Omega_{tip}U_r = \Omega_{tail}\frac{3\mu_s}{r}. \quad (19)$$

Assuming $d_{tip} \propto r$ and $d_{tail} \sim r$ as before, Ω_{tip} and Ω_{tail} can be calculated and substituted into Eq. 19. Also, by assuming $U_r \propto U_0$, Eq. 19 can be transformed into

$$Re \sim \beta, \quad (20)$$

where β is a constant. For $Re \lesssim \beta$, a no-pinch-off jet is expected to occur because the viscosity prevents the jet extension, and for $Re \gtrsim \beta$, a pinch-off jet is expected to occur because the inertial force is sufficient.

To confirm that the elasticity of the solution does not affect the jet behavior in this viscous dominated region, we investigated the jet behavior of a Newtonian fluid, aqueous-

glycerin solution (G70W30) where the density ρ , viscosity μ_s , and surface tension σ of the glycerin solution are $\rho = 1175.4 \text{ kg/m}^3$, $\mu_s = 0.0169 \text{ Pa}\cdot\text{s}$, and $\sigma = 68.4 \text{ mN/m}$, respectively. Note that we do not consider the effect of the surface tension on the jet behavior since the surface tension for all viscoelastic and newtonian liquids are similar ($\sigma = 62.0\text{-}72.5 \text{ mN/m}$). Figure 7 shows a typical image of a G70W30 jet. As shown in Figure 7a, when $Re \sim 370$, the jet is pinched off at the tip after extension and a pinch-off jet is generated. On the other hand, when $Re \sim 230$, as shown in Figure 7b, the jet returns to the initial interface without being pinched off after ejection, so a no-pinch-off jet is generated. We determined from the experiments that the jet behaviors of the Newtonian fluid transitioned from no-pinch-off to pinch-off at $Re \sim 250$ (Figure 7). Therefore, in Eq. 20, the β obtained from the experiments is $\beta \sim 250$, and the threshold for the occurrence of pinch-off jets in the region of $Wi \lesssim 10$ is

$$Re \gtrsim 250. \quad (21)$$

In Figure 5, the no-pinch-off and pinch-off jets can be generally distinguished using Eq. 18 (solid line) and Eq. 21 (dashed line). Therefore, it is evident that the jet behavior can be classified through modeling with the FENE-CR model.

Conclusions

In this study, we have conducted systematic experiments on jet behaviors in the high-viscoelasticity and high-velocity regime, which have not been investigated before. We generated a focused jet using polymer solution with a wide range of viscoelasticities and observed two characteristic behaviors: 1) The jet elongates and after a certain amount of time, the tip gets pinched off (pinch-off jet) and 2) The jet returns to the initial interface without pinch-off (no-pinch-off jet). The no-pinch-off jet in the highly elastic region gets pulled back after a large elongation. This phenomenon has been observed as a bungee-jumper jet in previous studies,^{16,23} but this study shows that the bungee-jumper jet is observed not only

in low-velocity regimes but also in the higher velocity and higher elasticity regime. We suggest that these jet behaviors can be reasonably classified using Reynolds number Re and Weissenberg number Wi , which are dimensionless numbers composed of the initial conditions of the jet ejection and the rheological properties of the solution. Furthermore, to understand this phenomenon we used a viscoelastic model, the FENE-CR model, and rationalized the experimental results.

We believe that this study provides significant insight into the viscoelasticity of jets with a focused geometry. This work will be useful for clarifying the effects of viscoelasticity on the breakup processes of various liquid jets in high-velocity regimes.

Acknowledgement

This work was funded by the Japan Society for the Promotion of Science (Grant Nos. 20H00223, 20H00222, and 20K20972), the Japan Science and Technology Agency PRESTO (Grant No. JPMJPR2105), and Japan Agency for Medical Research and Development (Grant No. JP22he0422016).

Conflict of interest

The authors declare no conflict of interest.

References

- (1) Eggers, J.; Villermaux, E. Physics of liquid jets. *Rep. Prog. Phys.* **2008**, *71*, 036601.
- (2) Tagawa, Y.; Oudalov, N.; Visser, C. W.; Peters, I. R.; van der Meer, D.; Sun, C.; Prosperetti, A.; Lohse, D. Highly Focused Supersonic Microjets. *Phys. Rev. X* **2012**, *2*, 031002.

- (3) Peters, I. R.; Tagawa, Y.; Oudalov, N.; Sun, C.; Prosperetti, A.; Lohse, D.; van der Meer, D. Highly focused supersonic microjets: numerical simulations. *J. Fluid Mech.* **2013**, *719*, 587–605.
- (4) Kiyama, A.; Tagawa, Y.; Ando, K.; Kameda, M. Effects of a water hammer and cavitation on jet formation in a test tube. *J. Fluid Mech.* **2016**, *787*, 224–236.
- (5) Worthington, A. M. *A study of splashes*; Longmans, Green, and Company: London, 1908.
- (6) Zeff, B. W.; Kleber, B.; Fineberg, J.; Lathrop, D. P. Singularity dynamics in curvature collapse and jet eruption on a fluid surface. *Nature* **2000**, *403*, 401–404.
- (7) Antkowiak, A.; Brémond, N.; Dizes, S. L.; Villiermaux, E. Short-term dynamics of a density interface following an impact. *J. Fluid Mech.* **2007**, *577*, 241 – 250.
- (8) Baxter, J.; Mitragotri, S. Needle-free liquid jet injections: mechanisms and applications. *Expert Rev. Med. Devices* **2006**, *3*, 565–574, PMID: 17064242.
- (9) Onuki, H.; Oi, Y.; Tagawa, Y. Microjet Generator for Highly Viscous Fluids. *Phys. Rev. Appl.* **2018**, *9*, 014035.
- (10) Gordillo, J. M.; Onuki, H.; Tagawa, Y. Impulsive generation of jets by flow focusing. *J. Fluid Mech.* **2020**, *894*, A3.
- (11) Zhang, Y.; Hu, G.; Liu, Y.; Wang, J.; Yang, G.; Li, D. Suppression and Utilization of Satellite Droplets for Inkjet Printing: A Review. *Processes* **2022**, *10*.
- (12) Lohse, D. Fundamental Fluid Dynamics Challenges in Inkjet Printing. *Annu. Rev. Fluid Mech.* **2022**, *54*, 349–382.
- (13) Delrot, P.; Modestino, M. A.; Gallaire, F. m. c.; Psaltis, D.; Moser, C. Inkjet Printing of Viscous Monodisperse Microdroplets by Laser-Induced Flow Focusing. *Phys. Rev. Appl.* **2016**, *6*, 024003.

- (14) Clasen, C.; Eggers, J.; Fontelos, M. A.; Li, J.; McKinley, G. H. The beads-on-string structure of viscoelastic threads. *J. Fluid Mech.* **2006**, *556*, 283–308.
- (15) McIlroy, C.; Harlen, O. G.; Morrison, N. F. Modelling the jetting of dilute polymer solutions in drop-on-demand inkjet printing. *J. Nonnewton Fluid Mech.* **2013**, *201*, 17–28.
- (16) Morrison, N. F.; Harlen, O. G. Viscoelasticity in inkjet printing. *Rheol. Acta* **2010**, *49*, 619–632.
- (17) Bazilevskii, A. V.; Meyer, J. D.; Rozhkov, A. N. Dynamics and Breakup of Pulse Microjets of Polymeric Liquids. *Fluid Dyn.* **2005**, *40*, 376–392.
- (18) Hoath, S. D.; Harlen, O. G.; Hutchings, I. M. Jetting behavior of polymer solutions in drop-on-demand inkjet printing. *J. Rheol.* **2012**, *56*, 1109–1127.
- (19) Sen, U.; Datt, C.; Segers, T.; Wijshoff, H.; Snoeijer, J. H.; Versluis, M.; Lohse, D. The retraction of jetted slender viscoelastic liquid filaments. *J. Fluid Mech.* **2021**, *929*, A25.
- (20) Turkoz, E.; Stone, H. A.; Arnold, C. B.; Deike, L. Simulation of impulsively induced viscoelastic jets using the Oldroyd-B model. *J. Fluid Mech.* **2021**, *911*, A14.
- (21) Turkoz, E.; Perazzo, A.; Kim, H.; Stone, H. A.; Arnold, C. B. Impulsively Induced Jets from Viscoelastic Films for High-Resolution Printing. *Phys. Rev. Lett.* **2018**, *120*, 074501.
- (22) Bousfield, D.; Keunings, R.; Marrucci, G.; Denn, M. Nonlinear analysis of the surface tension driven breakup of viscoelastic filaments. *J. Nonnewton Fluid Mech.* **1986**, *21*, 79–97.
- (23) Hoath, S.; Hutchings, I.; Martin, G.; Tuladhar, T.; Mackley, M.; Vardillo, D. Links between ink rheology, drop-on-demand jet formation, and printability. *J. Imaging Sci. Technol.* **2009**, *53*, 041208.

- (24) Torres, P.; Fonte, C. Flow regimes of a single pulse of inelastic and elastic liquids from a round capillary tube. *Chem. Eng. Sci.* **2022**, *248*.
- (25) Franco-Gómez, A.; Onuki, H.; Yokoyama, Y.; Nagatsu, Y.; Tagawa, Y. Effect of liquid elasticity on the behaviour of high-speed focused jets. *Exp. Fluids* **2021**, *62*, 1–15.
- (26) Kamamoto, K.; Kiyama, A.; Tagawa, Y.; Zhang, X. Ouzo Column under Impact: Formation of Emulsion Jet and Oil-Lubricated Droplet. *Langmuir* **2021**, *37*, 2056–2064.
- (27) Yukisada, R.; Kiyama, A.; Zhang, X.; Tagawa, Y. Enhancement of Focused Liquid Jets by Surface Bubbles. *Langmuir* **2018**, *34*, 4234–4240.
- (28) Gaillard, A.; Roché, M.; Lerouge, S.; Gay, C.; Lebon, L.; Limat, L. Viscoelastic liquid curtains: experimental results on the flow of a falling sheet of polymer solution. *J. Fluid Mech.* **2019**, *873*, 358–409.
- (29) Dinic, J.; Biagioli, M.; Sharma, V. Pinch-off dynamics and extensional relaxation times of intrinsically semi-dilute polymer solutions characterized by dripping-onto-substrate rheometry. *J. Polym. Sci. B: Polym. Phys.* **2017**, *55*, 1692–1704.
- (30) Dinic, J.; Jimenez, L. N.; Sharma, V. Pinch-off dynamics and dripping-onto-substrate (DoS) rheometry of complex fluids. *Lab Chip* **2017**, *17*, 460–473.
- (31) Dinic, J.; Zhang, Y.; Jimenez, L. N.; Sharma, V. Extensional Relaxation Times of Dilute, Aqueous Polymer Solutions. *ACS Macro Lett.* **2015**, *4*, 804–808.
- (32) Sur, S.; Rothstein, J. Drop breakup dynamics of dilute polymer solutions: Effect of molecular weight, concentration, and viscosity. *J. Rheol.* **2018**, *62*, 1245–1259.
- (33) Anna, S. L.; McKinley, G. H. Elasto-capillary thinning and breakup of model elastic liquids. *J. Rheol.* **2001**, *45*, 115–138.

- (34) Mathues, W.; Formenti, S.; McIlroy, C.; Harlen, O. G.; Clasen, C. CaBER vs ROJER—Different time scales for the thinning of a weakly elastic jet. *J. Rheol.* **2018**, *62*, 1135–1153.
- (35) Entov, V.; Hinch, E. Effect of a spectrum of relaxation times on the capillary thinning of a filament of elastic liquid. *J. Nonnewton Fluid Mech.* **1997**, *72*, 31–53.
- (36) Chilcott, M. D.; Rallison, J. M. Creeping flow of dilute polymer solutions past cylinders and spheres. *J. Nonnewton Fluid Mech.* **1988**, *29*, 381–432.

TOC Graphic

